REVIEW ARTICLE

Compressed Sensing in Sodium Magnetic Resonance Imaging: Techniques, Applications, and Future Prospects

Qingping Chen, MSc,[1,2,3] N. Jon Shah, PhD,[1,4,5,6] and Wieland A. Worthoff, PhD[1]*

Sodium (^{23}Na) yields the second strongest nuclear magnetic resonance (NMR) signal in biological tissues and plays a vital role in cell physiology. Sodium magnetic resonance imaging (MRI) can provide insights into cell integrity and tissue viability relative to pathologies without significant anatomical alternations, and thus it is considered to be a potential surrogate biomarker that provides complementary information for standard hydrogen (^{1}H) MRI in a noninvasive and quantitative manner. However, sodium MRI suffers from a relatively low signal-to-noise ratio and long acquisition times due to its relatively low NMR sensitivity. Compressed sensing-based (CS-based) methods have been shown to accelerate sodium imaging and/or improve sodium image quality significantly. In this manuscript, the basic concepts of CS and how CS might be applied to improve sodium MRI are described, and the historical milestones of CS-based sodium MRI are briefly presented. Representative advanced techniques and evaluation methods are discussed in detail, followed by an expose of clinical applications in multiple anatomical regions and diseases as well as thoughts and suggestions on potential future research prospects of CS in sodium MRI.

Evidence Level: 5

Technical Efficacy: Stage 1

J. MAGN. RESON. IMAGING 2022;55:1340–1356.

Sodium (^{23}Na) is the second most abundant nucleus observable with magnetic resonance in biological tissues, surpassed only by the hydrogen nucleus (^{1}H). Sodium plays a pivotal role in the human body and has an important function in maintaining the homeostasis of organisms through osmoregulation and pH regulation.[1] In addition, it is involved in cell physiology through the regulation of sodium–potassium pumps, whose main purpose is to maintain the transmembrane sodium and potassium gradients by extruding three sodium ions from the cell while transferring two potassium ions into the cell and simultaneously consuming energy provided by adenosine triphosphate (ATP) hydrolysis.[2] The impairment of tissue energy metabolism or the disruption of cell membrane integrity causes an increase in intracellular sodium concentration (10–15 mmol/L), while the extracellular sodium concentration (140–150 mmol/L) remains constant due to tissue perfusion.[3–5] Therefore, a disturbance in the balance between intra- and extracellular sodium concentration is considered to be a sensitive early indicator of some diseases.[4] For example, when the activity of the sodium–potassium pumps is reduced due to insufficient ATP supply, for example, during ischemia,[6] the pumps cannot expel the influxive sodium properly, and thus an increase in intracellular sodium concentration can be observed.

Sodium magnetic resonance imaging (MRI) is the only noninvasive imaging technique that enables the absolute spatial quantification of sodium concentration in living tissues. It can provide direct biochemical information for cell integrity and tissue viability with little or no macroscopic alterations, making it useful for tracking temporal changes in tissue

View this article online at wileyonlinelibrary.com. DOI: 10.1002/jmri.28029

Received Oct 14, 2021, Accepted for publication Dec 3, 2021.

*Address reprint requests to: W.A.W., Institute of Neuroscience and Medicine 4, Forschungszentrum Jülich GmbH, 52425 Jülich, Germany. E-mail: w.worthoff@fz-juelich.de

From the [1]Institute of Neuroscience and Medicine 4, INM-4, Forschungszentrum Jülich GmbH, Jülich, Germany; [2]Faculty of Medicine, RWTH Aachen University, Aachen, Germany; [3]Department of Biomedical Engineering, The University of Melbourne, Parkville, Victoria, Australia; [4]Institute of Neuroscience and Medicine 11, INM-11, JARA, Forschungszentrum Jülich GmbH, Jülich, Germany; [5]JARA–BRAIN-Translational Medicine, Aachen, Germany; and [6]Department of Neurology, RWTH Aachen University, Aachen, Germany

viability during a course of treatment and giving it the potential to become a biomarker for early preventive diagnosis in clinical practice.[4] Initial demonstrations of the feasibility of sodium MRI in the human body date back to the early 1980s.[7,8] With the availability of stronger magnetic fields (≥3 T) as well as advancements in acquisition strategies and hardware, the potential of sodium MRI has been investigated in many recent studies across a variety of diseases, ranging from brain tumors,[9,10] multiple sclerosis,[11,12] stroke,[13] osteoarthritis,[14] and breast cancer,[15,16] to nephropathy,[17] and others.[4,5]

However, compared to conventional hydrogen MRI, sodium MRI has to surmount a number of hurdles if it is to enter routine clinical practice. In particular, the interrelated issues of relatively low signal-to-noise ratio (SNR) and long measurement times (usually exceeding 10 minutes) due to the low relative sensitivity of sodium nuclear magnetic resonance (NMR) compared to hydrogen (approximately 9.2%)[3] remain problematic, even when imaging is conducted at ultra-high fields.[18] These issues emerge from the fact that the gyromagnetic ratio of sodium is approximately 4-fold lower than that of hydrogen; the nuclear spin of sodium takes a value of 3/2 compared to 1/2 for hydrogen and hence exhibits a nuclear quadrupolar moment, and sodium concentration in vivo is approximately 2000 times lower than that of hydrogen. Furthermore, the interaction of the nuclear quadrupolar moment with the electric field gradients originating from the electronic distribution surrounding the nucleus in biological tissues results in a biexponential relaxation behavior, causing relatively fast decay of the sodium NMR signal.[19,20] A short transversal relaxation component, typically less than 5 msec, commonly constitutes about 60% of the signal, while the long component, typically ranging from 15 msec to 30 msec, contributes about 40% of the signal, favoring ultra-short echo time (UTE) imaging techniques for the detection of both components.[4] In contrast, the quadrupolar interaction is averaged to zero in a homogenous environment such as a fluid, and therefore the transverse relaxation of sodium NMR signal proceeds as a relatively slow mono-exponential decay.[4,19,20]

Fortunately, a variety of highly efficient acquisition techniques and delicate reconstruction approaches have been developed to enhance image quality and/or reduce the acquisition times of MRI scans by means of *k*-space undersampling. For example, parallel imaging can accelerate measurements with multichannel receiver coils by utilizing coil sensitivity variations in conjunction with a smaller number of gradient encoding steps.[21–23] However, the wide application of parallel imaging in sodium MRI is currently hindered by the limited availability of phased-array sodium-tuned coils. An alternative method applicable for accelerating single-channel coil scans is compressed sensing (CS), which is based on the principle that an image with a sparse representation in a known transform domain can be recovered from incoherently undersampled *k*-space data by means of a nonlinear iterative reconstruction.[24,25] MRI agrees well with this principle as MRI scanners naturally acquire the Fourier-encoded raw data instead of pixel samples and MRI images are naturally compressible in some transform domains. More importantly, due to the biexponential relaxation behavior with a fast T_2 value typically less than 5 msec in biological tissues, sodium MRI usually employs non-Cartesian UTE sampling schemes, such as radial[26] or spiral[27,28] acquisitions, achieving the incoherent undersampling required by CS. Ever since Madelin et al demonstrated the applicability of CS in sodium MRI in a study of human knee cartilage,[29] CS has been increasingly applied to sodium imaging of the brain,[30–32] skeletal muscle,[33,34] breasts,[15,35] and human torso.[36] Recent efforts have been made to further advance CS sodium MRI by incorporating methods such as dictionary-based learning,[36,37] prior hydrogen anatomical constraint,[32] parallel imaging,[38] or deep learning.[39] As an emerging technique, CS has great potential in further facilitating the clinical applicability of sodium MRI by, for example, applying advanced incoherent undersampling methods,[27,40,41] or by accelerating intracellular sodium mapping,[42,43] quantitative relaxometry,[9,10,44] and dynamic sodium MRI.[45,46]

Sodium MRI methods and applications have been extensively reviewed elsewhere,[4,5,47,48] and there are multiple reviews on the CS techniques and applications in hydrogen MRI.[49–53] However, to the best of the authors' knowledge, sodium MRI with the incorporation of CS has not yet been thoroughly reviewed. In light of the above, this article offers a review of CS-based sodium MRI over the last decade, focusing on advanced techniques, clinical applications, and potential future research prospects.

Basic Principles for the Application of Compressed Sensing to Sodium MRI

Biomedical images, for example, sodium MRI images, are naturally compressible with little or no perceptual loss of information. Conventionally, image compression is performed following image acquisition in order to save storage space and transfer time. The image content is transformed into a vector of sparse coefficients by compression tools, such as discrete cosine transform (DCT) or wavelet transform, and a standard compression strategy is used to encode the few significant coefficients and discard the most negligible or unimportant coefficients, thus enabling near-perfect reconstruction of the original data. As sodium MRI suffers from relatively low image quality and long measurement times, reducing measurement time without significant degradation of the image quality is crucial for sodium MRI to become clinically feasible. This naturally raises the following question: Can one directly measure only the compressed information in sodium MRI, while maintaining most of the reconstructed image quality? Note that the MRI system naturally acquires Fourier-encoded coefficients (i.e. *k*-space samples)

rather than pixels, DCT, or wavelet coefficients. The acquired demodulated signal in the MRI system is subject to the following form of Fourier integral:

$$s(t) \propto \int M_{xy}\left(\vec{r}, t=0\right) \cdot e^{-i\vec{k}(t).\vec{r}} d\vec{r}, \quad (1)$$

where $s(t)$ is the acquired MRI signal after demodulation, $\vec{r}$ is the coordinate of the spatial domain, $M_{xy}\left(\vec{r}, t=0\right)$ is the transverse magnetization of the object immediately after radiofrequency pulse excitation, and $\vec{k}(t)$ is the *k*-space coordinate.

Therefore, the above question can be restated: Is it possible to reconstruct sodium MRI images without significant visual loss by measuring a small subset of the *k*-space? Fortunately, the mathematical theory of CS published by Donoho[54] and Candès et al[24,25] clears the path for accelerated sodium MRI. According to the mathematical results, three ingredients are required for the application of CS to sodium MRI: 1) transform sparsity to separate and remove the noise from the desired image content, 2) incoherent undersampling to speed up data acquisition and avoid distinct aliasing artifacts, and 3) nonlinear iterative reconstruction to balance sparse representation of the desired image and data consistency of the acquired *k*-space data. As shown in Fig. 1, a sparse representation can be obtained by applying a sparsifying transform exemplified by a wavelet transform. A nonlinear iterative reconstruction is performed by leveraging, for example, the nonlinear conjugate gradient approach.[55] An image is updated in the $(i+1)$th iteration by feeding a conjugate gradient, which contains the information of the *i*th sparse domain as well as the difference between the measured *k*-space and the *i*th *k*-space, thus promoting image sparsity and data consistency. When the conjugate gradient or the number of iterations reaches the stopping criteria set by the user, the iteration loop is broken, and the final image is produced. The following subsections discuss the three fundamental requirements for the implementation of CS to sodium MRI in more detail.

Transform Sparsity

A vector can be said to be "sparse" provided that most of its coefficients are equal to zero and only a few coefficients contain all of the information. From a signal processing perspective, most energy from a sparse signal is contained within a few measurements, while the remaining measurements are zero or negligible. In mathematical terms, transform sparsity produces a sparse vector after a specific mathematical transformation and can be defined as follows: If an unknown signal with m samples is a vector, $x \in \mathbb{C}^m$, which can be expressed in terms of an orthonormal basis set $(\psi_i: i = 1, \ldots, m)$ for $\mathbb{C}^m$ (e.g. orthonormal wavelet basis), as follows:

$$\theta_i = \psi_i x,\ i = 1, \ldots, m \text{ or } \theta = \Psi x \quad (2)$$

where $\theta \in \mathbb{C}^m$ is the transform coefficient set of x; the orthonormal basis set $(\psi_i: i = 1, \ldots, m)$ in matrix form, $\Psi \in \mathbb{C}^{m \times m}$, is also called sparsifying transform operator.

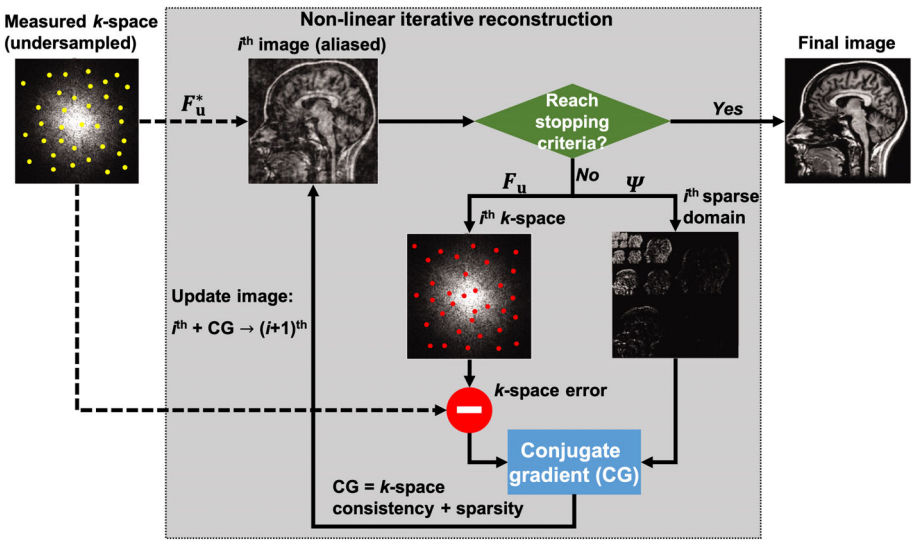

FIGURE 1: A simplified schematic of the fundamentals of compressed sensing. Randomly undersampled *k*-space datasets are acquired (top left); their inverse Fourier transformation results in an image with incoherent artifacts. A sparse representation is obtained by employing wavelet transform. The gray box shows a nonlinear iterative reconstruction using a nonlinear conjugate gradient method. An image is updated by feeding a conjugate gradient, which is calculated based on *k*-space consistency and sparse domain information. When the conjugate gradient or the number of iterations reaches a set stopping criteria, the iteration loop is broken, and the final image is produced. F_u: undersampled Fourier transform operator, F_u^*: inverse undersampled Fourier transform operator, Ψ: sparsifying transform operator. *Source*: Figure reproduced from reference 55, with permission from John Wiley and Sons (License No. 5147660427238).

Then, the signal, x, is said to be k-sparse if only k elements of θ are nonzeroes ($k \ll m$), while the remaining $(m-k)$ elements are zeroes (as shown in Fig. 2a).

Sparsifying transform projects an image into a sparse domain based on a number of transform coefficients, thus suggesting the number of measurements required for an exact reconstruction. However, choosing the right transform tool to exploit sparsity for a particular class of MRI images is a challenging task and an ongoing research area. Fixed sparsifying transform operators are frequently employed in sodium MRI, such as wavelets,[30] finite differences,[15,33,37] or the orthogonal DCT.[30] Moreover, it is possible to perform sparse representation of sodium images based on a trained dictionary,[33,34,36,37] or others.[33,39]

Incoherent Undersampling

An essential requirement for CS is that the aliasing artifacts produced by k-space undersampling due to the Nyquist constraint violation are incoherent (i.e. noise-like) in the image domain since it is impossible to distinguish between signal and aliasing in the case of the undersampling not being random. In light of the fast biexponential relaxation behavior of the sodium nucleus, non-Cartesian UTE k-space trajectories are usually employed in sodium MRI, such as 3D radial,[56] stack of spirals,[57] density-adapted 3D projection,[58] twisted projection imaging (TPI),[40,41] flexible TPI,[59] 3D cones,[60] and Fermat looped, and orthogonally encoded trajectories (FLORET).[27] Generally, incoherent undersampling is achieved by randomly skipping a subset of phase-encode lines in Cartesian sampling or projections in non-Cartesian sampling (as shown in Fig. 3), such as variable-density sampling schemes,[61,62] leading to a reduction in MRI scan times. The artifacts produced by incoherent undersampling show a noise-like behavior in the image domain and even more so in an appropriately selected sparse domain. It has been reported that 3D non-Cartesian sampling, such as FLORET (Fig. 3f), provides better sparsity and hence yields greater CS performance than traditional 2D Cartesian sampling with incoherently undersampled phase-encodes and fully sampled readouts (Fig. 3a). This makes 3D non-Cartesian sampling an excellent candidate for CS-based reconstruction.[49,55]

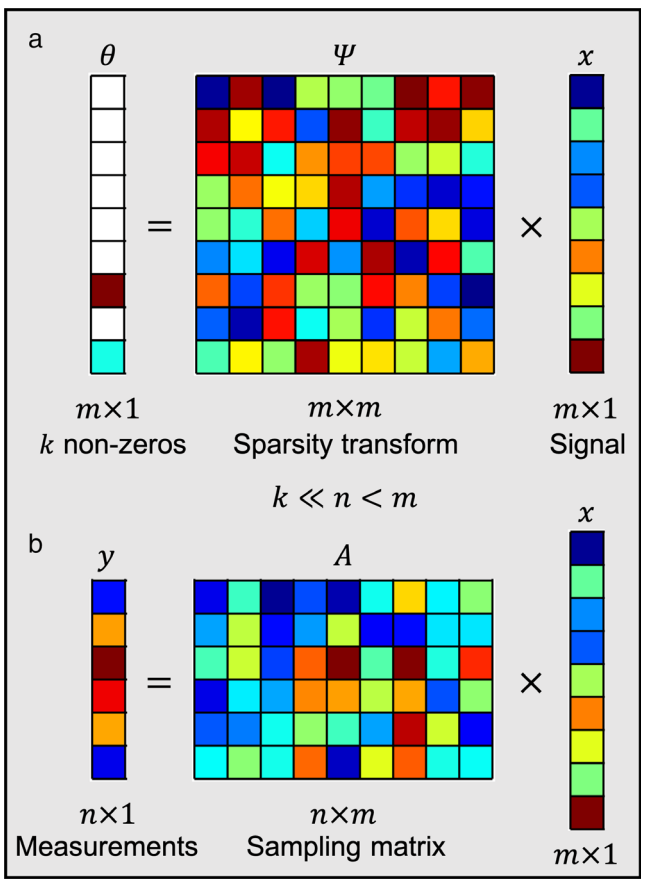

FIGURE 2: Basic principles of sparse representations. (a) Transform sparsity produces a set of sparse transform coefficients, θ, with k non-zero elements after a sparsifying transform, Ψ, operating on a signal, x. (b) An $m \times 1$ k-sparse signal can be transformed into an $n \times 1$ set of measurements, y, through an $n \times m$ sampling matrix, A ($k \ll n < m$). The colors represent the values of the elements in the matrices. The elements of θ in white are zeros.

Nonlinear Iterative Reconstruction

In the case of the undersampling described above, only n linear measurements ($n < m$) of the unknown signal, $x \in \mathbb{C}^m$, with m samples, are acquired and can be expressed in the following form:

$$y_i = a_i x,\ i = 1, \ldots, n \text{ or } y = Ax, \tag{3}$$

where $a_i \in \mathbb{C}^m$ is a known sampling vector in the ith measurement; $A \in \mathbb{C}^{n \times m}$ is the sampling matrix of dimension $n \times m$; and $y \in \mathbb{C}^n$ is the measured dataset with n samples from n measurements by applying the sampling matrix, A. A more intuitive interpretation of undersampling is shown in Fig. 2b. Of particular interest is the exact recovery of signal x in the vastly undersampled case, where the number of unknowns (m) is much larger than that of the observations (n), which might seem impossible at first glance. Candès et al[24,25,63] proposed that the signal of interest, x, can be exactly recovered by solving the ℓ_1-convex problem:

$$\min_x \|x\|_1 \text{ subject to } y = Ax, \tag{4}$$

where the ℓ_1-norm is the sum of the magnitudes of vector x, provided that the sampling matrix, A, has the restricted isometry property.[25] More specifically, for a given restricted isometry constant, δ_{2k}, a sampling matrix, A, is said to have a k-restricted isometry property if it satisfies the following condition for all k-sparse vectors x_1 and x_2 for $\mathbb{C}^m$:

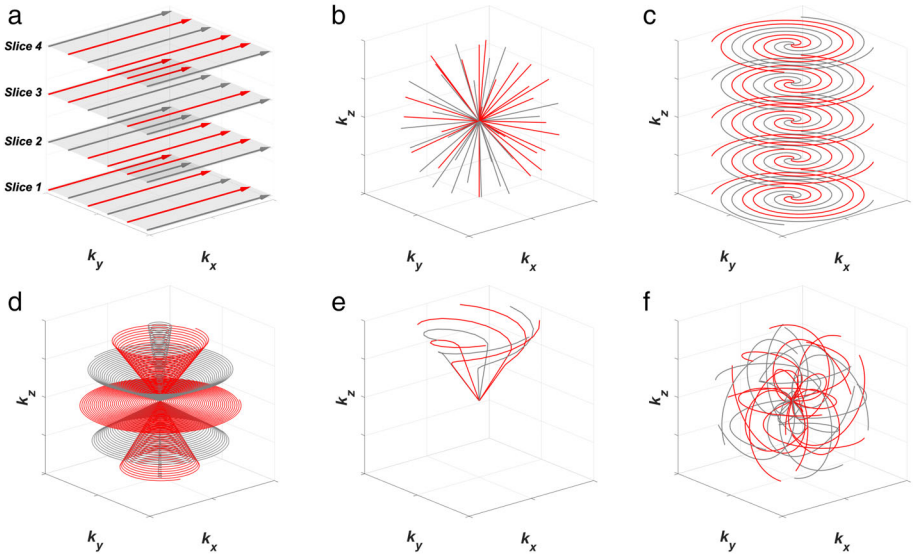

FIGURE 3: ***k*-space trajectories with 2-fold incoherent undersampling. Phase-encodes or projections in gray are skipped, while red ones are sampled. (a) 2D Cartesian trajectories with incoherently undersampled phase-encodes and fully sampled readouts. (b–f) 3D non-Cartesian UTE *k*-space trajectories often used in sodium MRI: (b) 3D radial, (c) stack of spirals, (d) 3D cones, (e) twisted projection imaging, and (f) Fermat looped, orthogonally encoded trajectories.**

$$(1-\delta_{2k})\|x_1-x_2\|_2^2 \le \|Ax_1-Ax_2\|_2^2 \le (1+\delta_{2k})\|x_1-x_2\|_2^2. \quad (5)$$

It has been found that there is a high probability of satisfying the requirements of the restricted isometry property if the undersampling pattern is incoherent and if the number of measurements is above a given constant that is determined according to the number of samples, m, and the sparsity value, k.[63]

In clinical practice, the signal x is usually projected into a specific domain to increase its sparsity as much as possible, thereby reducing the number of unknowns to achieve near-optimum image reconstruction, as shown in the following unconstrained formula adapted from Eq. 4:

$$\hat{x} = \arg\min_x \left\{ \|\Psi x\|_1 + \lambda \|y - Ax\|_2^2 \right\}, \quad (6)$$

where x is the iteratively generated image, $\hat{x}$ is the reconstructed image, y is the acquired k-space data, A is the Fourier transform operator, Ψ is the sparsifying transform operator such that Ψx becomes sparse, and λ is the regularization parameter to balance the ℓ_1-norm and ℓ_2-norm. Minimizing the ℓ_1-norm of the transform coefficients promotes sparsity, while the ℓ_2-norm constraint of the measured data ensures data consistency. In other words, out of all the potential solutions consistent with the measured data, Eq. 6 finds one that is compressible by transform Ψ. In addition, it is well-documented that the total variation (TV) norm, which is essentially the ℓ_1-norm of the variations of neighboring pixels or voxels, can promote image restoration because the finite difference operator can play a role as an edge-preserving filter to smooth regions with constant intensity.[64] Thus, to enforce the image sparsity both in the transform domain and in the finite-difference domain, a certain amount of TV penalty can be added to Eq. 6, as follows:

$$\hat{x} = \arg\min_x \left\{ \alpha TV(x) + \|\Psi x\|_1 + \lambda \|y - Ax\|_2^2 \right\}, \quad (7)$$

where α is the weighing factor for the TV penalty.

In addition to the aforementioned three fundamental requirements, there are several practical limitations and/or considerations when applying CS to sodium MRI. One of the limitations is that sodium MRI has relatively weak image sparsity due to the high noise contamination of sodium images. The concept of compressibility is introduced to quantify image sparsity, which is defined as the percentage of specified transform coefficients required to generate an image comparable to the fully sampled original image. It has been reported that the hydrogen images of the human head can be compressed up to 1.6%, while the corresponding sodium images only provide a compressibility of 72%.[65] In light of this, advanced techniques are often employed to promote the sparsity of sodium images. Second, center-out non-Cartesian sampling schemes often used in sodium MRI for incoherent undersampling require rapid switching of gradients and are therefore sensitive to hardware system imperfection. This can result in eddy currents, gradient delays, and related artifacts. Finally, CS has the potential to improve SNR and/or image resolution, whereas this may result in the loss of low-contrast features. Hence, the trade-off between these two factors must be taken into consideration.

Historical Milestones

Five years after Lustig et al demonstrated the applicability of CS in hydrogen MRI for the first time,[55] Madelin et al proved the applicability of CS in sodium MRI by successfully halving the scan time required for imaging knee cartilage at 7 T without significant loss of accuracy in total sodium concentration (TSC).[29] Although CS sodium MRI is still considered an emerging technique, it has made significant progress in the past decade, as shown in the list of publications given in Table 1, which is, to the best of our knowledge, a complete list of all publications relating to CS-based sodium MRI to this date. Following the work of Madelin et al,[29] Gnahm et al optimized the CS sodium MRI technique by combining its TV regularization with prior high-resolution anatomical information from hydrogen MRI, resulting in a substantial increase in SNR and enhanced contrast of structures in the sodium MRI images.[31,32] In addition to the standard ℓ_1-norm and TV penalty, several innovative sparsity regularizations have been employed for the application of CS to sodium MRI, such as second-order TV and dictionary-based learning.[15,37,68,70] Lachner et al pioneered the combination of parallel imaging with CS sodium MRI in a study on female breast imaging using a multichannel phased-array

TABLE 1. Publications Relating to Compressed Sensing-Based Sodium MRI

Year	Publication	Sampling Scheme	Regularization	USF	B_0 (T)	Anatomical Region
2012	Madelin et al[29]	3D radial	No sparsifying transform (one subject: DCT)	2	7	Knee cartilage (asymptomatic)
2014	Gnahm et al[32]	DA-3DPR	TV with anatomical prior	2	3	Brain (healthy)
2015	Weingärtner et al[65]	CSI	Anatomical prior with phase homogeneity constraint	3	3	Brain (ischemic stroke)
2015	Maguire et al[66]	CSI	Wavelet, TV	3	9.4	Mouse heart
2015	Gnahm et al[31]	DA-3DPR	TV with anatomical prior	4	7	Brain (multiple sclerosis)
2016	Behl et al[37]	DA-3DPR	TV, DL	9	7	Brain (healthy)
2018	Platt et al[36]	DA-3DPR	DL	1	7	Human torso (healthy)
2019	Blunck et al[30]	3D radial	TV, wavelet, DCT	4	7	Brain (healthy)
2019	Lachner et al[15]	DA-3DPR	TV with anatomical prior	7.2	7	Female breasts (healthy)
2020	Utzschneider et al[34]	DA-3DPR	DL	4.4	3	Skeletal muscle (healthy)
2020	Regnery et al[67]	DA-3DPR	DL	-	7	Brain (glioma)
2020	Lachner et al[38]	DA-3DPR	TV with SENSE and anatomical prior	7.2	7	Female breasts (healthy)
2020	Kratzer et al[68]	2D DA radial	DL	21	7	Brain (healthy)
2021	Utzschneider et al[33]	DA-3DPR, DA-SOS	TV, DL, TV-BL	4.1	7	Skeletal muscle (healthy)
2021	Adlung et al[39]	DA-3DPR	Convolutional neural networks	4	7	Brain (ischemic stroke)
2021	Zhao et al[69]	Flexible TPI	TV with anatomical prior	1	3	Brain (healthy and high-grade tumor)
2021	Kratzer et al[70]	3D DA radial	DL	2	7	Brain (healthy)

USF = undersampling factor for acceptable image quality; DCT = discrete cosine transform; DA-3DPR = density-adapted 3D radial; TV = total variation; CSI = chemical shift imaging; DL = dictionary-based learning; SENSE = sensitivity encoding; DA radial = density-adapted radial; DA-SOS = 3D acquisition-weighted density-adapted stack-of-stars sampling scheme; TV-BL = total variation CS with 4D block-matching prior; TPI = twisted projection imaging.

sodium/hydrogen double-tuned coil and found that the incorporation of parallel imaging improved CS reconstruction with higher image quality.[38] More recently, Adlung et al provided proof for the first time that convolutional neural networks in the field of deep learning were able to reconstruct 4-fold undersampled sodium MRI images with loss functions acting as regularizations while maintaining SNR and TSC quantification accuracy for ischemic stroke patients.[39] The majority of the research relating to CS-based sodium MRI have been conducted at an ultra-high field strength of 7 T using various forms of 3D radial sampling schemes with undersampling factors (USFs) ranging from 2 to 10. The effects of sparse reconstruction on the quantitation of TSC and relaxometry have been investigated in multiple studies.[30,34,39,68–70] Further to UTE sequences using non-Cartesian *k*-space trajectories, the chemical shift imaging (CSI) sequence[71] without readout gradients was shown to be a feasible modality for CS sodium MRI by Weingärtner et al, by using iterative reconstruction with the aid of an object support constraint from hydrogen MRI and a phase-homogeneity constraint.[65] Furthermore, Maguire et al demonstrated the capability of CS to accelerate sodium magnetic resonance spectroscopic imaging using a CSI sequence, achieving 3-fold acceleration without losing accuracy of the myocardial sodium concentration maps for mouse hearts in vivo at 9.4 T.[66]

Advanced Techniques in Compressed Sensing-Based Sodium MRI

Although the benefits of conventional CS have been demonstrated in terms of shortening the scan times and/or improving image quality in sodium MRI, many challenges impede its full potential and limit its clinical translation. First, conventional CS typically demands complex iterative algorithms for solving non-linear optimization problems, resulting in clinically infeasible computational times (usually in hours). Second, the manually chosen transform domain, such as wavelet or finite difference, may not accurately model the sparse representation of the target data, therefore leading to artifacts. Finally, conventional CS reconstruction performance is sensitive to the tuning of extensive regularization parameters that heavily depend on the type of image, sparsifying transform, sampling trajectories, patients, and so on, making the manual tuning of parameters a difficult task in practice. In the following, four advanced techniques to mitigate these challenges and thus to improve the performance of CS in sodium MRI are introduced in detail.

Dictionary-Based Learning

A dictionary is essentially a matrix of values that can be employed as a sparsifying transform in a CS reconstruction. Common sparsifying transforms, such as wavelet, DCT, and finite difference, have a fixed and analytic form of dictionary and work by employing an orthonormal basis set, enabling fast and straightforward implementation of CS by zeroing out most of the transform coefficients. However, these transforms are only suitable for a specific class of signals in the MRI data at best and do not optimally represent other signals due to the involved simplistic and rigid sparsifying algorithms. Consequently, data-adapted (i.e. learned) transforms are essential for dealing with a vast range of signals. These can yield sparser representations than fixed transforms since their dictionaries are learned separately for every image instance.[72,73] Common dictionary-based learning techniques include patch-based methods[74] and magnetic resonance fingerprinting (MRF).[75]

Ravishankar and Bresler proposed a novel framework for the application of patch-based dictionary-based learning to hydrogen MRI, which can learn the dictionary iteratively and simultaneously reconstruct the MRI image from highly undersampled *k*-space data.[74] Behl et al introduced this framework to sodium MRI and extended the dimensionality of the dictionary patch from 2D to 3D within acceptable reconstruction times in light of the relatively low image resolution of sodium MRI.[37] In the context of sodium MRI, the following minimization problem based on Eq. 7 has to be solved iteratively:

$$\left\{\widehat{D},\widehat{\alpha}_{\mathrm{ijk}},\widehat{x}\right\}=\underset{D,\alpha_{\mathrm{ijk}},x}{\arg\min}\left\{\sum_{\mathrm{ijk}}\mu_{\mathrm{ijk}}\left\|\alpha_{\mathrm{ijk}}\right\|_0+\sum_{\mathrm{ijk}}\left\|D\alpha_{\mathrm{ijk}}-R_{\mathrm{ijk}}x\right\|_2^2+\lambda\|y-Ax\|_2^2\right\}, \tag{8}$$

where $x\in\mathbb{C}^{\mathrm{N}\times 1}$ is the iteratively reconstructed image of size $\sqrt[3]{N}\times\sqrt[3]{N}\times\sqrt[3]{N}$ voxels, A is the Fourier transform operator, and y is the measured *k*-space data. $R_{\mathrm{ijk}}\in\mathbb{C}^{\mathrm{n}\times\mathrm{N}}$ is an operator that extracts a patch of interest from image x as $x_{\mathrm{ijk}}=R_{\mathrm{ijk}}x$ of size $\sqrt[3]{n}\times\sqrt[3]{n}\times\sqrt[3]{n}$ voxels. $\alpha_{\mathrm{ijk}}\in\mathbb{C}^{\mathrm{K}\times 1}$ is a sparse representation of the image patch, $x_{\mathrm{ijk}}\in\mathbb{C}^{\mathrm{n}\times 1}$, with respect to the dictionary, $D\in\mathbb{C}^{\mathrm{n}\times\mathrm{K}}$, $K\ll N$. The first term

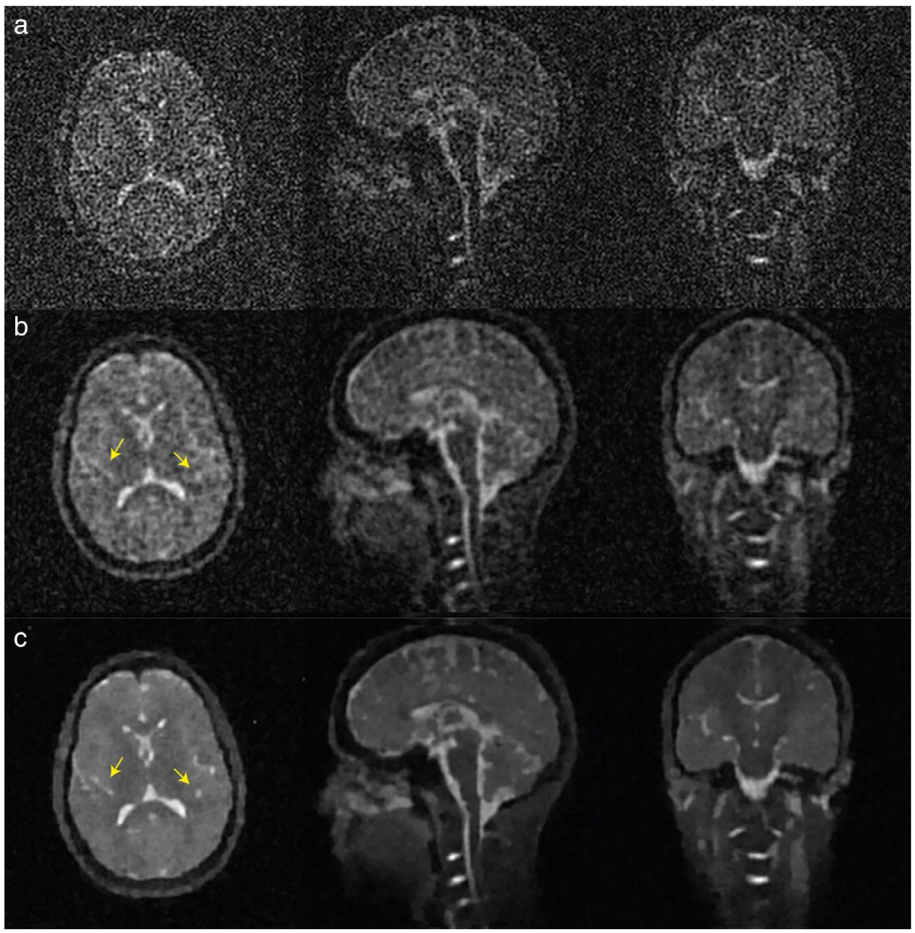

FIGURE 4: Sodium MRI images of a healthy human brain with a nominal resolution of 1.7 mm^3 reconstructed using (a) NUFFT, (b) CS with a TV regularization, and (c) the adaptive 3D dictionary-based CS algorithm. The raw data were acquired with a USF of 9 and an average of 5. The adapted 3D dictionary-based learning CS is less affected by noise and can restore small structures more accurately than other reconstruction approaches (eg in the cerebellum). *Source*: Figure reproduced from reference 37, with permission from John Wiley and Sons (License No. 5147660846875).

promotes the sparsity of the dictionary-based patch representation, α_{ijk}, where the ℓ_0-norm, $\|\alpha_{ijk}\|_0$, is the total number of nonzero elements in vector α_{ijk}. The second term enforces the consistency of the reconstructed image patch, $R_{ijk}x$, and its dictionary-based approximation, $D\alpha_{ijk}$. The third term ensures the data fidelity in k-space. Behl et al showed that the 3D patch-based dictionary-based learning reconstruction is superior to the conventional nonuniform fast Fourier transform (NUFFT) and other CS reconstructions using nonadaptive sparsifying transforms (eg finite difference).[37] This is especially the case for moderate undersampling (Fig. 4) and is in line with another study on imaging the skeletal muscles of healthy volunteers using a USF of 4.1 by Utzschneider et al.[33]

MRF, a recently proposed dictionary-based approach, produces a unique signal evaluation (i.e. fingerprint) from various tissues or materials by employing an incoherently undersampled acquisition, which is matched to a predefined dictionary of predicted signal evaluations for multiparametric quantification in hydrogen MRI.[75] In accordance with patch-based dictionary-based learning, the idea of MRF is that a single element in a sparse set of dictionary elements can be used to represent the time course of each pixel, depending on relaxometry and other parameters. Kratzer et al first proved the feasibility of MRF in the simultaneous quantification of sodium relaxometry and B_0 inhomogeneity within 1 h in a preliminary study[68] and further halved the scan time to achieve time-efficient 3D in vivo relaxometric mapping.[70]

The transition from nonadapted image sparsity to adapted dictionary-based sparsity is attractive for sodium MRI since the adapted dictionaries can capture small image features and remove artifacts effectively without sacrificing image resolution. However, this comes at the expense of a highly nonconvex optimization problem, which is often associated with high computational complexity and long reconstruction times due to challenging theoretical analyses and convergence guarantees. Although the previously trained dictionary might be reutilized, each reconstruction task has to solve a new optimization problem, resulting in a great computational burden.

Combination of Hydrogen Anatomical Information

Hydrogen MRI can provide an excellent SNR and a high resolution within a relatively short measurement time and is often used to complement non-hydrogen MRI measurements by providing anatomical references. Thus, there is naturally great interest in employing hydrogen anatomical information to improve the image quality of nonhydrogen MRI since MRI images of the same body part obtained with different MRI contrasts are highly correlated due to the same underlying anatomy. Constantinides et al first proposed an iterative reconstruction algorithm to enhance low-resolution sodium MRI by incorporating high-resolution hydrogen MRI before the onset of CS.[76] While CS exploits the sparsity of non-hydrogen MRI images to accelerate data acquisition, incorporating prior anatomical knowledge from hydrogen MRI into the CS reconstruction algorithm provides further opportunities to improve image quality for non-hydrogen MRI, such as phosphorus (^{31}P),[77] hyperpolarized helium (^{3}He),[78] and fluorine (^{19}F).[79] Gnahm et al first introduced this concept to CS sodium MRI by using a hydrogen support region constraint[32] and further advanced it by adding an edge-weighting-based constraint[31] to exploit hydrogen anatomical information. Accordingly, the constrained optimization problem of CS (Eq. 7) is rewritten as:

$$\hat{x} = \arg\min_{x}\left\{\lambda_1\|y - Ax\|_2^2 + \lambda_2 \sum_{\alpha=x,y,z}\left(\tau\left\|W_\alpha D_\alpha^{(1)}x\right\|_1 + (1-\tau)\left\|W_\alpha D_\alpha^{(2)}x\right\|_1\right) + \lambda_3\|BM\cdot x\|_2^2\right\} \quad (9)$$

where x is the iteratively generated image and $\hat{x}$ is the reconstructed image. λ_1, λ_2, and λ_3 are the weighing factors of data consistency constraint, edge-weighting-based anatomical constraint, and support region constraint, respectively. $D_\alpha^{(i)}$ denotes the derivative operator computing the ith-order TV in α direction,[80] weighted by τ. The second-order TV, $D_\alpha^{(2)}$, is used to avoid patchy images because the first-order TV, $D_\alpha^{(1)}$, tends to generate regions with constant intensity.[80,81] W_α is the diagonal matrix containing anatomical weighting factors ranging from 0 to 1 and is derived from $D_\alpha^{(1)}$ of a registered and normalized hydrogen MRI reference image in α direction. BM is the diagonal matrix obtained from a hydrogen image with 1 outside the object region and 0 inside. ℓ_2-norm instead of ℓ_1-norm is used in the third term to minimize the signal intensities outside of the object, leading to an increase in image quality.

However, in the presence of sodium-dependent novel features (e.g. abnormality invisible in the hydrogen image), the approach indicated in Eq. 9 can only achieve minimal improvement in reconstructing these novel features and is sensitive to interscan subject motion. To address these issues, Zhao et al proposed an anatomically constrained reconstruction approach for sodium MRI that enables denoising and resolution enhancement of shared features between hydrogen and sodium images, meanwhile allowing motion correction and recovery of the novel features that are present only in sodium images (Fig. 5).[69] The CS with hydrogen anatomical constraints was shown to outperform NUFFT and the conventional CS without hydrogen anatomical constraints. Moreover, it was shown to be particularly effective when the hydrogen image reference shared similar structures with the sodium image.[15,31,32,38,69]

It should be noted that the hydrogen anatomical information that is not contained in sodium dataset can introduce artificial structures to the reconstructed sodium images. Thus, it is critical that only reliable prior information is used for the anatomical incorporation, such as object support region and lesions.

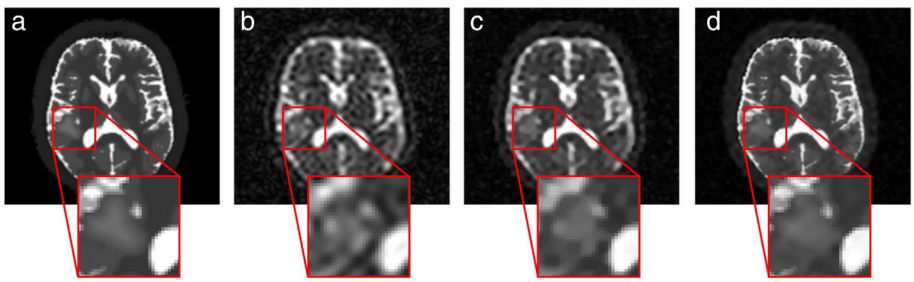

FIGURE 5: Simulated sodium MRI images with a lesion. (a) Ground truth image. (b–d) Images after adding complex Gaussian noise reconstructed by (b) NUFFT, (c) conventional CS without anatomical constraints, and (d) CS with anatomical constraints. *Source*: Figure reproduced from reference 69, with permission from John Wiley and Sons (License No. 5147661032006).

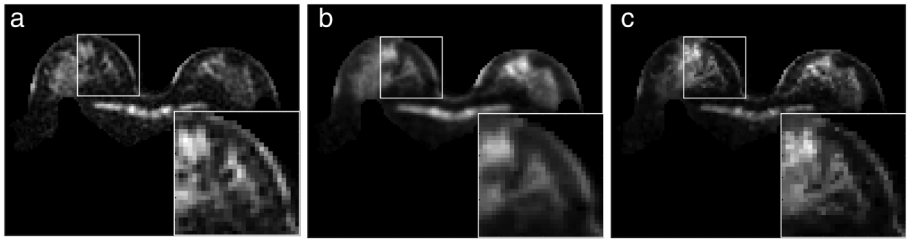

FIGURE 6: Sodium images of healthy female breasts with a USF of 7.2 at 7 T. Three images were reconstructed by (a) NUFFT, (b) CS without SENSE, and (c) SENSE-based CS. Compared to NUFFT reconstruction. Both CS-based results show significant improvement because of reduced noise and artifacts as well as resolved structures. In contrast to the CS algorithm without SENSE, the SENSE-based CS algorithm yields further improvement due to the reduced blurring and well-preserved small structures. *Source*: Figure reproduced from reference 38, with permission from Elsevier (License No. 5147661364797).

Combination of Parallel Imaging

Parallel imaging is an MRI acceleration technique that exploits the properties of phased-array coils[82] to assist the spatial localization of the multichannel NMR signal sampled below the Nyquist sampling rate.[83] Two representative parallel imaging techniques are used routinely in the clinic: SENSitivity Encoding (SENSE)[21] and GeneRalised Partially Parallel Acquisitions (GRAPPA).[23] SENSE unfolds aliased pixels in the image domain by using the prior knowledge of coil sensitivity profiles. GRAPPA synthesizes missing data points directly in *k*-space as a linear combination of the acquired neighboring *k*-space points by implicitly employing the coil sensitivity information calculated from a densely sampled center region of the *k*-space data. Inspired by the high accessibility of hydrogen-tuned phased-array coils, as well as the similar purpose of parallel imaging and CS, extensive research work has been carried out to synergistically combine the two for further acceleration of hydrogen MRI.[84–90] In light of the increasing applications of sodium-tuned phased-array coils,[28,35,91,92] the combination of parallel imaging and CS in sodium MRI to obtain faster scans and/or higher image quality has aroused great interest. Lachner et al first proposed an augmented CS reconstruction algorithm for sodium MRI by utilizing the estimated coil sensitivity profiles.[38] Given the coil sensitivity for C channels: S_i, $\mathrm{i}=1,\ldots,C$, this algorithm can be formulated as:

$$\widehat{x}=\arg\min_{x}\left\{\lambda\sum_{\mathrm{i}=1}^{C}\left\|S_\mathrm{i}\Phi x-y_\mathrm{i}\right\|_2^2+\sum_{\mathrm{i}}\tau_\mathrm{i}R_\mathrm{i}(x)\right\} \qquad (10)$$

where $\widehat{x}$ is the reconstructed image. The first term weighted with λ ensures data consistency with comparison to the acquired *k*-space data, y_i, of channel *i*. The matrix, Φ, projects the iteratively reconstructed image, x, into *k*-space for each channel, by multiplication with sensitivity maps S_i. The second term represents the incorporated regularizations, R_i, weighted with τ_i, to enforce image sparsity and/or introduce prior anatomical information. Lachner et al applied this SENSE-based CS algorithm to reconstruct 14-channel sodium breast datasets with a USF of 7.2, achieving further improvements in image quality compared to NUFFT and CS without SENSE (Fig. 6).[38]

In contrast to the hydrogen anatomical prior, parallel imaging always delivers reliable information to further improve CS performance by exploiting coil sensitivity profiles. Parallel imaging-based CS has shown encouraging results both in hydrogen[84–90] and sodium MRI.[38] However, its widespread use in sodium MRI is limited in practice due to the extreme lack of access to sodium-tuned phased-array coils, justifying the necessity of developing multichannel sodium-tuned coils in the future.

Incorporation of Deep Learning

Deep learning is a popular postprocessing technique that trains the brain-like multiple processing layers, known as artificial neural networks, to learn an off-line prior model from a large amount of historical data. Although, at first glance, deep learning might be regarded as a totally different technique from CS, recent work has shown that the fundamentals of deep learning are closely related to CS.[93] To address the challenges of CS, such as long computation times and difficult parameterization, CS has been recently extended to incorporate deep learning, enabling fast and accurate reconstruction of undersampled *k*-space data. Wang et al took the lead in applying deep learning to CS hydrogen MRI by training a convolutional neural network to obtain a mapping from retrospectively 5-fold undersampled to fully sampled *k*-space data.[94] This image reconstruction was achieved within 1 second. Lee et al adopted U-net,[95] a deep convolutional network consisting of a contracting path and an expansive path, to extract features of aliasing artifacts and therefore enable image reconstruction from sparsely sampled *k*-space data instantly.[96] Novel CS frameworks with high-efficient data consistency constraints were proposed by leveraging generative adversarial networks for rapid and accurate image reconstruction from highly undersampled MRI measurements.[97,98] Taking encouragement from the successes of deep learning-based CS in hydrogen MRI,[94,96–98] recent advances have also addressed sodium MRI.[39] Figure 7 illustrates an example development procedure for a deep learning framework for

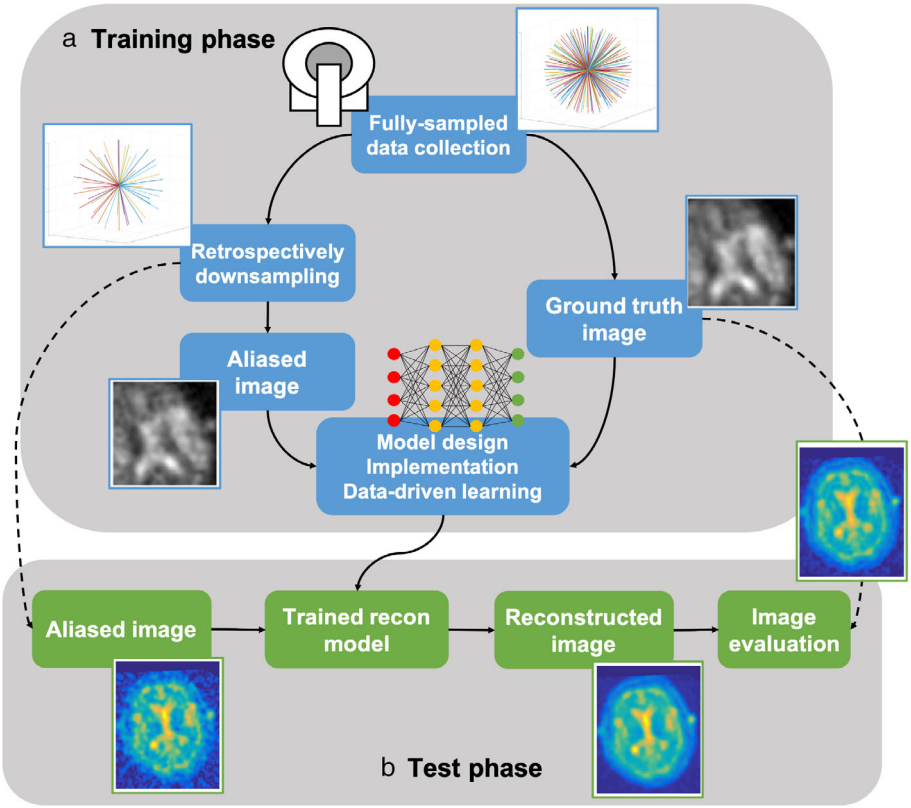

FIGURE 7: Diagrams showing an example development procedure for a deep learning framework for sodium MRI image reconstruction. Fully sampled *k*-space datasets are first collected and then divided into two parts for training and test. (a) The reconstruction algorithm is designed, built, and trained from a large number of training datasets. (b) The performance of the trained reconstruction model is evaluated in the test phase. *Source*: Figure reproduced from reference 39, with permission from John Wiley and Sons (License No. 5147670041968).

sodium image reconstruction.[39] Fully sampled *k*-space data sets are first collected and then randomly divided into two sets, a training set and a test set. The aliased images are produced by incoherent undersampling retrospectively. In the training phase, the reconstruction algorithm is designed, implemented, and trained by feeding a large number of training datasets. The test datasets are used to evaluate the performance of the final model by comparing the reconstructed images with the fully sampled ground truth images. The deep learning approach with convolutional neural networks based on a U-Net architecture was proven to achieve sufficiently accurate image reconstruction for 4-fold incoherently undersampled sodium MRI with a total computational time of less than 1 minute,[39] further advancing the real-time clinical application of sodium MRI.

Although incorporating deep learning into CS-based reconstruction techniques for sodium MRI shows encouraging results, several remaining challenges need to be addressed before it can be widely used in clinical practice. First of all, while CS has been proven to be a robust technique, deep learning-based reconstruction methods run the risk of introducing false information, especially in unique pathological situations. Furthermore, although it might be feasible to pretrain separate neural networks for different MRI exams, the poor generalization of deep learning in the case of, for example, different pulse sequence settings, MRI vendors, magnetic field strengths, anatomy, or pathologies, is an obstacle to its successful translation into clinical practice. Another major disadvantage lies in the availability of specific training and test datasets. The lack of a fully sampled dataset limits the use of deep learning models in supervised training. Thus, future research in an unsupervised training or scan-specific way by leveraging, for example, generative adversarial networks is anticipated.

Evaluation

Researchers are faced with a critical obstacle: the difficulty of evaluating the performance of various CS-based reconstruction techniques because the true evaluation of reconstruction is based on the diagnostic value of the reconstructed images, which clearly cannot be identified in a development cycle. Thus, the undermentioned quantitative and qualitative methods, as well as statistical analysis, are often used as proxies.

The quantitative method is implemented to calculate image metrics by comparing resulting images with ground truth images obtained from fully sampled *k*-space data by applying the NUFFT algorithm. Common image metrics

include structural similarity (SSIM) based on degradation of structural information,[15,30,35,37,39,99] normalized root-mean-square error (NRMSE) for measurement of numerical similarity,[33,34,38,65] SNR difference to ground truth,[29,31,32,39,69] and peak SNR.[37] Furthermore, quantitative sodium MRI provides TSC that is connected to cellular integrity and viability.[3,4,100,101] Accordingly, the error of TSC to the ground truth can be used as an image metric unique to sodium MRI techniques.[33,39]

However, for the clinical establishment of a reconstruction technique, its ability to enable the visualization of specific pathologies and anatomical structures is much more important to radiologists than a mathematical match to a ground truth that might still be flawed. Therefore, a qualitative evaluation of clinical studies with blinded grading of image quality by multiple radiologists is recommended.[102] Image quality can be evaluated based on a set of criteria, including overall image quality, perceived SNR, image contrast, sharpness, residual artifacts, and diagnostic confidence, with specifically defined scores ranging from 1 (nondiagnostic) to 5 (excellent).[39,102,103] However, even this is a proxy for a true evaluation of diagnostic accuracy in clinical routine.

Provided that the number of consecutive scans is statistically meaningful (usually greater than 20), statistical analysis can be performed to show the statistical difference between two sets of images or two reconstruction approaches.[14] Since image metrics (e.g. SSIM and TSC error) regarding ground truth usually follow a normal distribution, a paired Student's t-test can be used to evaluate the statistical significance of image metrics obtained from two reconstruction techniques.[39] The difference in terms of image quality scores between two sets of images can be statistically assessed with a nonparametric statistical test, such as a Wilcoxon test, which can determine whether the scores of two different reconstructions come from the same distribution.[102] Ideally, a CS-based reconstruction algorithm for undersampled *k*-space data should draw results from a distribution same as that of ground truth images.

Clinical Applications

Sodium ion homeostasis in human biology is of great significance in ensuring the proper functioning of a cell, as exemplified by energy-consuming processes of membrane transport using the sodium–potassium pump.[5] Moreover, loss of homeostasis is often a sign of disorders, such as multiple sclerosis[11] and osteoarthritis.[14] Quantitative sodium MRI is a noninvasive way of providing novel biochemical markers that can be used to detect pathological processes at an early stage of the disease, benefitting diagnostic assessment, or for tracking changes in tissue viability in response to therapies, thus aiding treatment planning. Given these applications, the potential benefits of sodium MRI in clinical practice are clear. However, the reliable measurement of quantitative values with biological significance in the human body is compromised by a relatively low SNR, and the widespread clinical use of sodium MRI remains prohibitively expensive due to the long measurement times required to overcome this drawback.

The ultimate goal of a CS-based sodium MRI technique is to improve scanning speed and/or image quality for a particular application, such as brain imaging, musculoskeletal imaging, or cartilage imaging, while maintaining diagnostic accuracy. By leveraging in vivo datasets typically obtained from healthy volunteers and sometimes a small number of diseased subjects, the performance of the technique has been demonstrated in a small set of proof-of-concept reconstructions. This section briefly summarizes in vivo applications sorted by targeted anatomical regions or diseases, among which various CS-based sodium MRI techniques hold clinical promise.

The impacts of CS-based techniques on neuroimaging using sodium MRI have been investigated by multiple groups on healthy and/or diseased human brains.[30–32,37,39,65,67,69] Blunck et al probed the effects of conventional CS on quantitative sodium MRI on healthy human brains at 7 T by comparing three sparsity regularizations (Wavelet, DCT, and TV) over USFs ranging from 1 to 10.[30] It was found that CS enabled undersampling up to a factor of 4 while maintaining good image quality and high TSC quantification accuracy. In cerebral stroke events, the inadequate oxygen supply results in the energy-consuming failure of sodium-potassium pumps, therefore breaking sodium homeostasis across cell membranes. This leads to an increased TSC that can be measured by sodium MRI, albeit at the cost of relatively long scan times, to guide medical management decisions.[13,104,105] In studies of cerebral ischemic stroke using CS-based sodium MRI, a scan time reduction by moderate undersampling has been achieved with only minor degradation of image quality.[39,65] Similarly, multiple sclerosis lesions show an elevated TSC that might be the direct consequence of inflammatory and neurodegenerative processes. However, the metabolic basis for this remains unclear.[12,106,107] CS-based reconstruction approaches have been employed to accelerate sodium MRI examinations of multiple sclerosis while still preserving small anatomical structures and producing only little lesion intensity error that allows for relatively precise determination of TSC.[31] Brain tumors are included in the active role of sodium because the energy-consuming process of sodium–potassium pumps has a significant impact on tumor viability. An elevation in TSC appears in brain tumors due to the increase in intracellular sodium concentration and the enlargement of the extracellular space.[5,108] As shown in Fig. 8, the application of CS-based reconstruction has significantly improved the image quality of

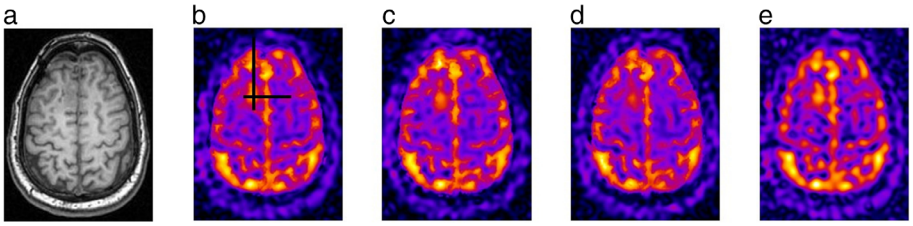

FIGURE 8: Hydrogen and sodium images of a brain tumor patient across radiation therapy. (a) Hydrogen MRI image on day 0 corresponding to the start of radiation treatment. (b–d) The TSC maps reconstructed with a CS-based method on (b) day 10, (c) day 24, and (d) day 45. (e) The TSC map reconstructed with NUFFT on day 10. The black crossing indicates the tumor location. The CS-based method (b) outperforms NUFFT (e) in terms of image quality of TSC maps. *Source*: Figure reproduced from reference 69, with permission from John Wiley and Sons (License No. 5147670179454).

TSC maps during the treatment of brain tumors. This indicates the potential to improve the detection of spatially heterogeneous responses of tumors to treatment.[69]

Consistent with brain tumors, breast cancers exhibit a significantly elevated TSC compared to glandular or fatty tissue.[16,109] Recent advances have shown that the application of CS-based techniques in breast sodium MRI can significantly shorten the acquisition time while preserving image quality.[15,38]

In skeletal muscle tissue, elevations in TSC have been reported in diseases, such as myotonic dystrophy,[110] muscular channelopathy,[111] diabetes,[112] and hypertension.[113] Acceleration of musculoskeletal sodium MRI by virtue of CS reconstruction with high quantification accuracy has also been demonstrated.[33,34]

Sodium imaging of cartilage holds clinical promise because it can facilitate the noninvasive quantification of glycosaminoglycan content, which plays a key role in cartilage homeostasis and is therefore considered as a potential biomarker for the clinical diagnosis of early osteoarthritis and the assessment of cartilage repair tissue.[114,115] A preliminary study has demonstrated that CS-based reconstruction can achieve faster, but still accurate, quantitative sodium imaging of knee cartilage at 7 T, motivating further research and technical advance in the field of CS sodium MRI.[29]

In the human torso, simultaneous sodium imaging of the lungs,[116] heart,[117,118] breasts,[16,109,119] kidneys,[17,120] and intervertebral discs[121] is of interest as it could provide invaluable insight into the metabolism in, for instance, lung cancer,[116] and acute kidney injury.[17] However, quantitative sodium torso MRI encounters additional challenges in terms of measurement times due to a large field of view and artifacts caused by cardiac pulsation and respiration. Fortunately, it has been shown that sparse reconstruction can significantly improve the image quality of human torso sodium images.[36]

Despite the great clinical potential, CS-based sodium MRI techniques have not been widely adopted because, in addition to the technical challenges such as long reconstruction times, significant clinical hurdles to extensive testing remain, not to mention the adoption of these methods. First of all, for complete validation of new imaging techniques, their diagnostic accuracy in clinical routine has to be demonstrated at a reduced measurement time, which is a time-consuming and challenging process. Second, the imaging community lacks experience with the artifacts caused by CS-based reconstructions, which means that technologists or radiologists may not be able to troubleshoot or even identify the artifacts, thus leading to failure in diagnosis. Finally, testing CS-based sodium MRI techniques against a clinical gold standard could be problematic due to the difficulties associated with repeating some clinical exams, especially dynamic contrast-enhanced series. Moreover, even if a repetition were technically feasible, performing additional scans in a clinical environment would be challenging due to the high cost of MRI examinations and/or time constraints.

Future Prospects

Although the feasibility of various CS-based reconstruction techniques in the field of sodium MRI has been demonstrated in many scenarios, CS-based sodium MRI is an emerging technique and remains an open area of interest to researchers with great potential for further technological advancement and clinical applications. In the following, potential future prospects of these techniques are discussed.

As previously stated, mapping intracellular sodium is of particular importance because it can reflect, for example, the function of sodium–potassium pumps, while extracellular sodium concentration is relatively insensitive to local changes within an organ due to tissue perfusion. Several approaches have been proposed for intracellular sodium weighted acquisitions in human biology, such as inversion-recovery techniques for suppression of the sodium signal from an aqueous environment,[122–124] and multiple-quantum filtering[125–129] based on the assumption that triple-quantum-coherence sodium NMR signal mostly originates from a restricted (mainly intracellular) environment.[19,20] Figure 9 presents the single- and triple-quantum-filtered sodium images on a brain tumor patient by applying an enhanced SISTINA technique.[9,10,44] The brain tumor shows increased signal in the single-quantum-filtered image and yet a decrease in the triple-quantum-filtered image, indicating that multiple-quantum filtering might have the potential to provide complementary

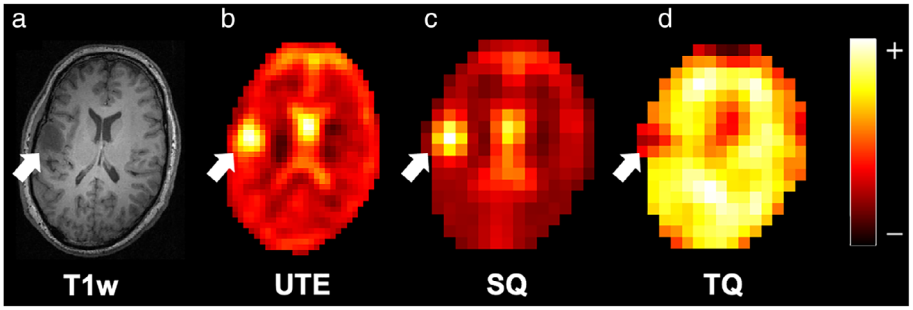

FIGURE 9: MRI images of a 33-year-old male patient with a brain tumor (white arrow). (a) The tumor shows little contrast enhancement in the T_1-weighted hydrogen MRI image. In sodium imaging with a total measurement time of about 10 minutes, the tumor shows (b) an increase in spin-density-weighted UTE signal, (c) an increase in single-quantum-filtered (SQ-filtered) sodium signal, (d) and a decrease in triple-quantum-filtered (TQ-filtered) sodium signal. Multiple-quantum-filtered sodium MRI adds information to the diagnosis of brain tumors.

information for diagnosis or medical treatment of some diseases. However, these techniques suffer from even longer acquisition times than conventional single-pulse sodium MRI due to their generally large specific absorption rate requirements, thus arousing interest in the acceleration of intracellular sodium mapping while maintaining image quality by using CS-based methods.

The electric quadrupole moment of the sodium nucleus under the effects of local electric field gradients can result in a biexponential transverse and longitudinal relaxation behavior, and studies have shown that certain pathologies, for example, brain tumors, can alter sodium relaxation times.[123,130] Consequently, the quantitation of sodium relaxometry might yield valuable additional information in the assessment of diffuse pathologies and potentially focal lesions. The sparse reconstruction of quantitative sodium relaxometry has been investigated using MRF, and a relatively long scan duration of 32 minutes has been reported for in vivo measurements, therefore limiting its clinical applications.[68,70] Hence, there is scope for CS-based techniques to efficiently accelerate quantitative sodium relaxometry.

Sodium dynamics have the potential to provide valuable information given the significant role of transmembrane sodium gradient in the regulation of neural activity and muscle action.[4] A dynamic sodium MRI technique to extract sub-30 seconds temporal information has been demonstrated but still suffers from a relatively long measurement time of 20 minutes.[45] Given the encouraging results of CS in speeding up dynamic hydrogen MRI, another important future prospect pertains to the acceleration of dynamic sodium MRI by leveraging, for example, k-t methods.[84,131]

As shown in Table 1, most of the CS sodium MRI studies to date have employed radial *k*-space trajectories for incoherent undersampling. Going forward, more efficient non-Cartesian *k*-space trajectories, such as TPI[40,41] or FLORET,[27] which have significantly higher SNR efficiency than radial trajectories, can be implemented for sparser representation of sodium MRI data, thus further accelerating sodium imaging times.

Conclusion

Sodium MRI is an excellent candidate for CS-based techniques because it naturally meets the fundamental requirements of CS in most cases, including transform sparsity and incoherent undersampling. Both conventional and advanced CS-based techniques have the potential to significantly accelerate sodium MRI scans and/or improve sodium image quality, thereby promoting the clinical applicability of sodium MRI. The performance of conventional CS can be further improved by introducing additional information, such as anatomical information obtained from hydrogen MRI, coil sensitivity information from phased-array coils, or by combining efficient sparse representation methods, for example, dictionary-based learning or deep learning. Given that the diagnostic value of reconstructed images cannot be assessed during the development cycle, proxies can be employed to evaluate the performance of various CS-based techniques, such as image metrics, subjective scoring, and statistical analysis. A variety of studies on multiple anatomical regions and diseases have shown the clinical potential of CS-based sodium MRI. Despite this, CS-based sodium MRI is still in its infancy, and many crucial issues remain unsettled before its widespread application in clinical routines. These include, but are not limited to: optimizing *k*-space sampling trajectories, developing improved sparse representation methods, investigating the reconstruction quality in terms of clinical significance, and shortening the reconstruction time. In the future, the clinical potential of CS-based sodium MRI could be further explored by, for example, accelerating the mapping of intracellular sodium, increasing the speed of relaxometry quantification, speeding up dynamic sodium MRI, and adopting advanced sampling schemes.

Acknowledgments

This work is considered to be part of the doctoral thesis (Dr. rer. medic.) of Qingping Chen at Faculty of Medicine,

RWTH Aachen University, Germany. Qingping Chen would like to thank Jülich-University of Melbourne Postgraduate Academy (JUMPA) for support and funding. The authors would like to express their sincere gratitude to Claire Rick and Nancy Malsbenden for their kind support.

References

1. Burnier M. *Sodium in health and disease*. 1st ed. New York: New Informa Healthcare USA, Inc; 2008. p 459.
2. Rose AM, Valdes RJ. Understanding the sodium pump and its relevance to disease. Clin Chem 1994;40:1674-1685.
3. Boada FE, LaVerde G, Jungreis C, Nemoto E, Tanase C, Hancu I. Loss of cell ion homeostasis and cell viability in the brain: What sodium MRI can tell us. Curr Top Dev Biol 2005;70:77-101.
4. Madelin G, Lee JS, Regatte RR, Jerschow A. Sodium MRI: Methods and applications. Prog Nucl Magn Reson Spectrosc 2014;79:14-47.
5. Thulborn KR. Quantitative sodium MR imaging: A review of its evolving role in medicine. Neuroimage 2018;168:250-268.
6. Fuller W, Eaton P, Bell JR, Shattock MJ. Ischemia-induced phosphorylation of phospholemman directly activates rat cardiac Na/K ATPase. FASEB J 2004;18:197-199.
7. Maudsley AA, Hilal SK. Biological aspects of sodium-23 imaging. Br Med Bull 1984;40:165-166.
8. Hilal SK, Maudsley AA, Ra JB, et al. In vivo NMR imaging of sodium-23 in the human head. J Comput Assist Tomogr 1985;9:1-7.
9. Shymanskaya A, Worthoff WA, Stoffels G, et al. Comparison of [18F] Fluoroethyltyrosine PET and sodium MRI in cerebral gliomas: A pilot study. Mol Imaging Biol 2020;22:198-207.
10. Worthoff WA, Shymanskaya A, Lindemeyer J, Langen KJ, Shah NJ. Relaxometry and quantification in sodium MRI of cerebral gliomas: A FET-PET and MRI small-scale study. NMR Biomed 2020;33:e4361.
11. Petracca M, Vancea RO, Fleysher L, Jonkman LE, Oesingmann N, Inglese M. Brain intra- and extracellular sodium concentration in multiple sclerosis: A 7 T MRI study. Brain A J Neurol 2016;139:795-806.
12. Huhn K, Engelhorn T, Linker RA, Nagel AM. Potential of sodium MRI as a biomarker for neurodegeneration and neuroinflammation in multiple sclerosis. Front Neurol 2019;10:84.
13. Boada FE, Qian Y, Nemoto E, et al. Sodium MRI and the assessment of irreversible tissue damage during hyper-acute stroke. Transl Stroke Res 2012;3:236-245.
14. Madelin G, Xia D, Brown R, et al. Longitudinal study of sodium MRI of articular cartilage in patients with knee osteoarthritis: Initial experience with 16-month follow-up. Eur Radiol 2018;28:133-142.
15. Lachner S, Zaric O, Utzschneider M, et al. Compressed sensing reconstruction of 7 tesla ^{23}Na multi-channel breast data using ^{1}H MRI constraint. Magn Reson Imaging 2019;60:145-156.
16. Zaric O, Farr A, Minarikova L, et al. Tissue sodium concentration quantification at 7.0-T MRI as an early marker for chemotherapy response in breast cancer: A feasibility study. Radiology 2021;299:63-72.
17. Hammon M, Grossmann S, Linz P, et al. 3 tesla 23Na magnetic resonance imaging during acute kidney injury. Acad Radiol 2017;24:1086-1093.
18. Ladd ME, Bachert P, Meyerspeer M, et al. Pros and cons of ultra-high-field MRI/MRS for human application. Prog Nucl Magn Reson Spectrosc 2018;109:1-50.
19. Jaccard G, Wimperis S, Bodenhausen G. Multiple-quantum NMR spectroscopy of S=3/2 spins in isotropic phase: A new probe for multiexponential relaxation. J Chem Phys 1986;85:6282-6293.
20. Rooney WD, Springer CSJ. A comprehensive approach to the analysis and interpretation of the resonances of spins 3/2 from living systems. NMR Biomed 1991;4:209-226.
21. Pruessmann KP, Weiger M, Scheidegger MB, Boesiger P. SENSE: Sensitivity encoding for fast MRI. Magn Reson Med 1999;42:952-962.
22. Sodickson DK, Manning WJ. Simultaneous acquisition of spatial harmonics (SMASH): Fast imaging with radiofrequency coil arrays. Magn Reson Med 1997;38:591-603.
23. Griswold MA, Jakob PM, Heidemann RM, et al. Generalized autocalibrating partially parallel acquisitions (GRAPPA). Magn Reson Med 2002;47:1202-1210.
24. Candès EJ, Romberg J, Tao T. Robust uncertainty principles: Exact signal reconstruction from highly incomplete frequency information. IEEE Trans Inf Theory 2006;52:489-509.
25. Candès EJ, Romberg JK, Tao T. Stable signal recovery from incomplete and inaccurate measurements. Commun Pure Appl Math 2006;59:1207-1223.
26. Matthies C, Nagel AM, Schad LR, Bachert P. Reduction of B0 inhomogeneity effects in triple-quantum-filtered sodium imaging. J Magn Reson 2010;75:239-244.
27. Pipe JG, Zwart NR, Aboussouan EA, Robison RK, Devaraj A, Johnson KO. A new design and rationale for 3D orthogonally oversampled k-space trajectories. Magn Reson Med 2011;66:1303-1311.
28. Qian Y, Stenger VA, Boada FE. Parallel imaging with 3D TPI trajectory: SNR and acceleration benefits. Magn Reson Imaging 2009;27:656-663.
29. Madelin G, Chang G, Otazo R, Jerschow A, Regatte RR. Compressed sensing sodium MRI of cartilage at 7T: Preliminary study. J Magn Reson 2012;214:360-365.
30. Blunck Y, Kolbe SC, Moffat BA, Ordidge RJ, Cleary JO, Johnston LA. Compressed sensing effects on quantitative analysis of undersampled human brain sodium MRI. Magn Reson Med 2019;83:1025-1033.
31. Gnahm C, Nagel AM. Anatomically weighted second-order total variation reconstruction of 23Na MRI using prior information from 1H MRI. Neuroimage 2015;105:452-461.
32. Gnahm C, Bock M, Bachert P, Semmler W, Behl NGR, Nagel AM. Iterative 3D projection reconstruction of ^{23}Na data with an ^{1}H MRI constraint. Magn Reson Med 2014;71:1720-1732.
33. Utzschneider M, Müller M, Gast LV, et al. Towards accelerated quantitative sodium MRI at 7 T in the skeletal muscle: Comparison of anisotropic acquisition- and compressed sensing techniques. Magn Reson Imaging 2021;75:72-88.
34. Utzschneider M, Behl NGR, Lachner S, et al. Accelerated quantification of tissue sodium concentration in skeletal muscle tissue: Quantitative capability of dictionary learning compressed sensing. Magn Reson Mater Physics, Biol Med 2020;33:495-505.
35. Lachner S, Ruck L, Niesporek SC, et al. Comparison of optimized intensity correction methods for ^{23}Na MRI of the human brain using a 32-channel phased array coil at 7 tesla. Z Med Phys 2020;30:104-115.
36. Platt T, Umathum R, Fiedler TM, et al. In vivo self-gated 23Na MRI at 7 T using an oval-shaped body resonator. Magn Reson Med 2018;80:1005-1019.
37. Behl NGR, Gnahm C, Bachert P, Ladd ME, Nagel AM. Three-dimensional dictionary-learning reconstruction of ^{23}Na MRI data. Magn Reson Med 2016;75:1605-1616.
38. Lachner S, Utzschneider M, Zaric O, et al. Compressed sensing and the use of phased array coils in 23Na MRI: A comparison of a SENSE-based and an individually combined multi-channel reconstruction. Z Med Phys 2020;31:48-57.
39. Adlung A, Paschke NK, Golla AK, et al. 23Na MRI in ischemic stroke: Acquisition time reduction using postprocessing with convolutional neural networks. NMR Biomed 2021;34:e4474.
40. Boada FE, Gillen JS, Shen GX, Chang SY, Thulborn KR. Fast three dimensional sodium imaging. Magn Reson Med 1997;37:706-715.
41. Boada FE, Shen GX, Chang SY, Thulborn KR. Spectrally weighted twisted projection imaging: Reducing T2 signal attenuation effects in fast three-dimensional sodium imaging. Magn Reson Med 1997;38:1022-1028.

42. Hancu I, Boada FE, Shen GX. Three-dimensional triple-quantum-filtered 23Na imaging of in vivo human brain. Magn Reson Med 1999; 42:1146-1154.

43. Fiege DP, Romanzetti S, Mirkes CC, Brenner D, Shah NJ. Simultaneous single-quantum and triple-quantum-filtered MRI of ^{23}Na (SISTINA). Magn Reson Med 2013;69:1691-1696.

44. Worthoff WA, Shymanskaya A, Shah NJ. Relaxometry and quantification in simultaneously acquired single and triple quantum filtered sodium MRI. Magn Reson Med 2019;81:303-315.

45. Bydder M, Zaaraoui W, Ridley B, et al. Dynamic ^{23}Na MRI - a non-invasive window on neuroglial-vascular mechanisms underlying brain function. Neuroimage 2019;184:771-780.

46. Grist JT, Riemer F, Hansen ESS, et al. Visualization of sodium dynamics in the kidney by magnetic resonance imaging in a multi-site study. Kidney Int 2020;98:1174-1178.

47. Shah NJ, Worthoff WA, Langen KJ. Imaging of sodium in the brain: A brief review. NMR Biomed 2016;29:162-174.

48. Zaric O, Juras V, Szomolanyi P, et al. Frontiers of sodium MRI revisited: From cartilage to brain imaging. J Magn Reson Imaging 2021;54:58-75.

49. Lustig M, Donoho DL, Santos JM, Pauly JM. Compressed sensing MRI. IEEE Signal Process Mag 2008;25:72-82.

50. Jaspan ON, Fleysher R, Lipton ML. Compressed sensing MRI: A review of the clinical literature. Br J Radiol 2015;88:20150487.

51. Yang ACY, Kretzler M, Sudarski S, Gulani V, Seiberlich N. Sparse reconstruction techniques in MRI: Methods, applications, and challenges to clinical adoption. Invest Radiol 2016;51:349-364.

52. Bustin A, Fuin N, Botnar RM, Prieto C. From compressed-sensing to artificial intelligence-based cardiac MRI reconstruction. Front Cardiovasc Med 2020;7:17.

53. Ye JC. Compressed sensing MRI: A review from signal processing perspective. BMC Biomed Eng 2019;1:8.

54. Donoho DL. Compressed sensing. IEEE Trans Inf Theory 2006;52: 1289-1306.

55. Lustig M, Donoho D, Pauly JM. Sparse MRI: The application of compressed sensing for rapid MR imaging. Magn Reson Med 2007;58: 1182-1195.

56. Nielles-Vallespin S, Weber MA, Bock M, et al. 3D radial projection technique with ultrashort echo times for sodium MRI: Clinical applications in human brain and skeletal muscle. Magn Reson Med 2007;57: 74-81.

57. Mirkes C, Shajan G, Bause J, Buckenmaier K, Hoffmann J, Scheffler K. Triple-quantum-filtered sodium imaging at 9.4 Tesla. Magn Reson Med 2016;75:1278-1289.

58. Nagel AM, Laun FB, Weber MA, Matthies C, Semmler W, Schad LR. Sodium MRI using a density-adapted 3D radial acquisition technique. Magn Reson Med 2009;62:1565-1573.

59. Lu A, Atkinson IC, Claiborne TC, Damen FC, Thulborn KR. Quantitative sodium imaging with a flexible twisted projection pulse sequence. Magn Reson Med 2010;63:1583-1593.

60. Gurney PT, Hargreaves BA, Nishimura DG. Design and analysis of a practical 3D cones trajectory. Magn Reson Med 2006;55:575-582.

61. Marseille GJ, De Beer R, Fuderer M, Mehlkopf AF, Van Ormondt D. Nonuniform phase-encode distributions for MRI scan time reduction. J Magn Reson - Ser B 1996;111:70-75.

62. Greiser A, von Kienlin M. Efficient k-space sampling by density-weighted phase-encoding. Magn Reson Med 2003;50:1266-1275.

63. Candes EJ, Tao T. Decoding by linear programming. IEEE Trans Inf Theory 2005;51:4203-4215.

64. Rudin LI, Osher S, Fatemi E. Nonlinear total variation based noise removal algorithms. Phys D Nonlinear Phenom 1992;60:259-268.

65. Weingärtner S, Wetterling F, Konstandin S, Fatar M, Neumaier-Probst E, Schad LR. Scan time reduction in ^{23}Na-magnetic resonance imaging using the chemical shift imaging sequence: Evaluation of an iterative reconstruction method. Z Med Phys 2015;25:275-286.

66. Maguire ML, Geethanath S, Lygate CA, Kodibagkar VD, Schneider JE. Compressed sensing to accelerate magnetic resonance spectroscopic imaging: Evaluation and application to ^{23}Na-imaging of mouse hearts. J Cardiovasc Magn Reson 2015;17:45.

67. Regnery S, Behl NGR, Platt T, et al. Ultra-high-field sodium MRI as biomarker for tumor extent, grade and IDH mutation status in glioma patients. NeuroImage Clin 2020;28:102427.

68. Kratzer FJ, Flassbeck S, Nagel AM, et al. Sodium relaxometry using 23Na MR fingerprinting: A proof of concept. Magn Reson Med 2020; 84:2577-2591.

69. Zhao Y, Guo R, Li Y, Thulborn KR, Liang ZP. High-resolution sodium imaging using anatomical and sparsity constraints for denoising and recovery of novel features. Magn Reson Med 2021;86:625-636.

70. Kratzer FJ, Flassbeck S, Schmitter S, et al. 3D sodium (23Na) magnetic resonance fingerprinting for time-efficient relaxometric mapping. Magn Reson Med 2021;86:2412-2425.

71. Brown TR, Kincaid BM, Ugurbil K. NMR chemical shift imaging in three dimensions. Proc Natl Acad Sci U S A 1982;79:3523-3526.

72. Elad M, Aharon M. Image denoising via sparse and redundant representations over learned dictionaries. IEEE Trans Image Process 2006; 15:3736-3745.

73. Ravishankar S, Bresler Y. Efficient blind compressed sensing using sparsifying transforms with convergence guarantees and application to magnetic resonance imaging. SIAM J Imaging Sci 2015;8:2519-2557.

74. Ravishankar S, Bresler Y. MR image reconstruction from highly undersampled k-space data by dictionary learning. IEEE Trans Med Imaging 2011;30:1028-1041.

75. Ma D, Gulani V, Seiberlich N, et al. Magnetic resonance fingerprinting. Nature 2013;495:187-192.

76. Constantinides CD, Weiss RG, Lee R, Bolar D, Bottomley PA. Restoration of low resolution metabolic images with a priori anatomic information: ^{23}Na MRI in myocardial infarction. Magn Reson Imaging 2000;18:461-471.

77. Rink K, Benkhedah N, Berger MC, et al. Iterative reconstruction of radially-sampled 31P bSSFP data using prior information from 1H MRI. Magn Reson Imaging 2017;37:147-158.

78. Ajraoui S, Parra-Robles J, Wild JM. Incorporation of prior knowledge in compressed sensing for faster acquisition of hyperpolarized gas images. Magn Reson Med 2013;69:360-369.

79. Obert AJ, Gutberlet M, Kern AL, et al. 1H-guided reconstruction of 19F gas MRI in COPD patients. Magn Reson Med 2020;84:1336-1346.

80. Block KT, Uecker M, Frahm J. Undersampled radial MRI with multiple coils. Iterative image reconstruction using a total variation constraint. Magn Reson Med 2007;57:1086-1098.

81. Geman D, Yang C. Nonlinear image recovery with half-quadratic regularization. IEEE Trans Image Process 1995;4:932-946.

82. Roemer PB, Edelstein WA, Hayes CE, Souza SP, Mueller OM. The NMR phased array. Magn Reson Med 1990;16:192-225.

83. Deshmane A, Gulani V, Griswold MA, Seiberlich N. Parallel MR imaging. J Magn Reson Imaging 2012;36:55-72.

84. Jung H, Sung K, Nayak KS, Kim EY, Ye JC. k-t FOCUSS: A general compressed sensing framework for high resolution dynamic MRI. Magn Reson Med 2009;61:103-116.

85. Lustig M, Pauly JM. SPIRiT: Iterative self-consistent parallel imaging reconstruction from arbitrary k-space. Magn Reson Med 2010;64: 457-471.

86. Otazo R, Kim D, Axel L, Sodickson DK. Combination of compressed sensing and parallel imaging for highly accelerated first-pass cardiac perfusion MRI. Magn Reson Med 2010;64:767-776.

87. Liang D, Liu B, Wang J, Ying L. Accelerating SENSE using compressed sensing. Magn Reson Med 2009;62:1574-1584.

88. Jung H, Ye JC, Kim EY. Improved k-t BLAST and k-t SENSE using FOCUSS. Phys Med Biol 2007;52:3201-3226.

89. Deka B, Datta S. Calibrationless joint compressed sensing reconstruction for rapid parallel MRI. Biomed Signal Process Control 2020;58:101871.

90. Seo N, Park MS, Han K, et al. Feasibility of 3D navigator-triggered magnetic resonance cholangiopancreatography with combined parallel imaging and compressed sensing reconstruction at 3T. J Magn Reson Imaging 2017;46:1289-1297.

91. Malzacher M, Chacon-Caldera J, Paschke N, Schad LR. Feasibility study of a double resonant 8-channel 1 H/ 8-channel ^{23}Na receive-only head coil at 3 tesla. Magn Reson Imaging 2019;59:97-104.

92. Qian Y, Zhao T, Wiggins GC, et al. Sodium imaging of human brain at 7 T with 15-channel array coil. Magn Reson Med 2012;68:1807-1814.

93. Ye JC, Han Y, Cha E. Deep convolutional framelets: A general deep learning framework for inverse problems. SIAM J Imaging Sci 2018; 11:991-1048.

94. Wang S, Su Z, Ying L, et al. Accelerating magnetic resonance imaging via deep learning. *Proceedings of IEEE 13th international symposium on biomedical imaging*. Prague: IEEE; 2016. p 514-517.

95. Ronneberger O, Fischer P, Brox T. U-net: Convolutional networks for biomedical image segmentation. LNCS 2015;9351:234-241.

96. Lee D, Yoo J, Ye JC. Deep residual learning for compressed sensing MRI. *Proceedings of IEEE 14th international symposium on biomedical imaging*. Melbourne: IEEE; 2017. p 15-18.

97. Quan TM, Nguyen-Duc T, Jeong WK. Compressed sensing MRI reconstruction using a generative adversarial network with a cyclic loss. IEEE Trans Med Imaging 2018;37:1488-1497.

98. Mardani M, Gong E, Cheng JY, et al. Deep generative adversarial neural networks for compressive sensing MRI. IEEE Trans Med Imaging 2019;38:167-179.

99. Wang Z, Bovik AC, Sheikh HR, Simoncelli EP. Image quality assessment: From error visibility to structural similarity. IEEE Trans Image Process 2004;13:600-612.

100. Winkler SS. Sodium-23 magnetic resonance brain imaging. Neuroradiology 1990;32:416-420.

101. Thulborn KR, Lu A, Atkinson IC, Damen F, Villano JL. Quantitative sodium MR imaging and sodium bioscales for the management of brain tumors. Neuroimaging Clin N Am 2009;19:615-624.

102. Sandino CM, Cheng JY, Chen F, Mardani M, Pauly JM, Vasanawala SS. Compressed sensing: From research to clinical practice with deep neural networks. IEEE Signal Process Mag 2020;37: 117-127.

103. Chen F, Taviani V, Malkiel I, et al. Variable-density single-shot fast spin-echo MRI with deep learning reconstruction by using variational networks. Radiology 2018;289:366-373.

104. Jones SC, Kharlamov A, Yanovski B, et al. Stroke onset time using sodium MRI in rat focal cerebral ischemia. Stroke 2006;37:883-888.

105. Thulborn KR, Gindin TS, Davis D, Erb P. Comprehensive MR imaging protocol for stroke management: Tissue sodium concentration as a measure of tissue viability in nonhuman primate studies and in clinical studies. Radiology 1999;213:156-166.

106. Inglese M, Madelin G, Oesingmann N, et al. Brain tissue sodium concentration in multiple sclerosis: A sodium imaging study at 3 tesla. Brain A J Neurol 2010;133:847-857.

107. Zaaraoui W, Konstandin S, Audoin B, et al. Distribution of brain sodium accumulation correlates with disability in multiple sclerosis: A cross-sectional ^{23}Na MR imaging study. Radiology 2012;264:859-867.

108. Bruehlmeier M, Roelcke U, Blauenstein P, et al. Measurement of the extracellular space in brain tumors using 76Br-bromide and PET. J Nucl Med 2003;44:1210-1218.

109. Jacobs MA, Ouwerkerk R, Wolff AC, et al. Multiparametric and multinuclear magnetic resonance imaging of human breast cancer: Current applications. Technol Cancer Res Treat 2004;3: 543-550.

110. Constantinides CD, Gillen JS, Boada FE, Pomper MG, Bottomley PA. Human skeletal muscle: Sodium MR imaging and quantification - potential applications in exercise and disease. Radiology 2000;216:559-568.

111. Weber MA, Nagel AM, Marschar AM, et al. 7-T 35Cl and 23Na MR imaging for detection of mutation-dependent alterations in muscular edema and fat fraction with sodium and chloride concentrations in muscular periodic paralyses. Radiology 2016;281:326-337.

112. Chang G, Wang L, Schweitzer ME, Regatte RR. 3D ^{23}Na MRI of human skeletal muscle at 7 tesla: Initial experience. Eur Radiol 2010; 20:2039-2046.

113. Kopp C, Linz P, Dahlmann A, et al. ^{23}Na magnetic resonance imaging-determined tissue sodium in healthy subjects and hypertensive patients. Hypertension 2013;61:635-640.

114. Zbýň Š, Mlynárik V, Juras V, Szomolanyi P, Trattnig S. Evaluation of cartilage repair and osteoarthritis with sodium MRI. NMR Biomed 2016;29:206-215.

115. Madelin G, Babb J, Xia D, et al. Articular cartilage: Evaluation with fluid-suppressed 7.0-T sodium MR imaging in subjects with and subjects without osteoarthritis. Radiology 2013;268:481-491.

116. Henzler T, Konstandin S, Schmid-Bindert G, et al. Imaging of tumor viability in lung cancer: Initial results using 23Na-MRI. Rofo 2012;184: 340-344.

117. Graessl A, Ruehle A, Waiczies H, et al. Sodium MRI of the human heart at 7.0T: Preliminary results. NMR Biomed 2015;28:967-975.

118. Lott J, Platt T, Niesporek SC, et al. Corrections of myocardial tissue sodium concentration measurements in human cardiac 23Na MRI at 7 tesla. Magn Reson Med 2019;82:159-173.

119. Ouwerkerk R, Jacobs MA, Macura KJ, et al. Elevated tissue sodium concentration in malignant breast lesions detected with non-invasive 23Na MRI. Breast Cancer Res Treat 2007;106:151-160.

120. Zöllner FG, Konstandin S, Lommen J, et al. Quantitative sodium MRI of kidney. NMR Biomed 2016;29:197-205.

121. Insko EK, Clayton DB, Elliott MA. In vivo sodium MR imaging of the intervertebral disk at 4 T. Acad Radiol 2002;9:800-804.

122. Madelin G, Lee JS, Inati S, Jerschow A, Regatte RR. Sodium inversion recovery MRI of the knee joint in vivo at 7T. J Magn Reson 2010;207: 42-52.

123. Nagel AM, Amarteifio E, Lehmann-Horn F, et al. 3 tesla sodium inversion recovery magnetic resonance imaging allows for improved visualization of intracellular sodium content changes in muscular channelopathies. Invest Radiol 2011;46:759-766.

124. Stobbe R, Beaulieu C. In vivo sodium magnetic resonance imaging of the human brain using soft inversion recovery fluid attenuation. Magn Reson Med 2005;54:1305-1310.

125. Borthakur A, Hancu I, Boada FE, Shen GX, Shapiro EM, Reddy R. In vivo triple quantum filtered twisted projection sodium MRI of human articular cartilage. J Magn Reson 1999;141:286-290.

126. Tanase C, Boada FE. Triple-quantum-filtered imaging of sodium in presence of B0 inhomogeneities. J Magn Reson 2005;174:270-278.

127. Fleysher L, Oesingmann N, Inglese M. B0 inhomogeneity-insensitive triple-quantum-filtered sodium imaging using a 12-step phase-cycling scheme. NMR Biomed 2010;23:1191-1198.

128. Fiege DP, Romanzetti S, Tse DHY, et al. B0 insensitive multiple-quantum resolved sodium imaging using a phase-rotation scheme. J Magn Reson 2013;228:32-36.

129. Benkhedah N, Bachert P, Semmler W, Nagel AM. Three-dimensional biexponential weighted 23Na imaging of the human brain with higher SNR and shorter acquisition time. Magn Reson Med 2013;70:754-765.

130. Nagel AM, Bock M, Hartmann C, et al. The potential of relaxation-weighted sodium magnetic resonance imaging as demonstrated on brain tumors. Invest Radiol 2011;46:539-547.

131. Gamper U, Boesiger P, Kozerke S. Compressed sensing in dynamic MRI. Magn Reson Med 2008;59:365-373.